REDUCING UNCERTAINTIES IN THE VELOCITIES DETERMINED BY INVERSION OF PHASE VELOCITY DISPERSION CURVES USING SYNTHETIC SEISMOGRAMS

by

Seyed Mehrdad Hosseini

A Dissertation

Submitted in Partial Fulfillment of the

Requirements for the Degree of

Doctor of Philosophy

Major: Engineering

The University of Memphis

August 2014

Dedicated to my Mother, to the memory of my Father,

and to my Brothers, Mahmood and Mehran.

Acknowledgements

I would like to thank my supervisor, Dr. Shahram Pezeshk, for his dedication and support throughout the years of my academic endeavors. I will always appreciate your superior mentorship and endless patience that helped me accomplish my educational goals.

I also greatly appreciate Dr. Martin Chapman who answered my fundamental questions and generously helped me learn invaluable lessons from him and expand my scientific vision. I will always be grateful, thank you.

I also would like to thank my committee members, Professors Chris Cramer, Roger Meier, and Charles Camp for all their help in making this dissertation possible. I would like to express my gratitude for all you have done for me. Thank you.

I would like to thank my mother and brothers especially Mehran for his support during my studies. This work could not be possible without them. Your support is greatly appreciated and will never be forgotten.

At the end, I would also like to thank Ann Meier for her help in proofreading the dissertation, and Alireza Haji-Soltani for his help in formatting parts of the dissertation.

This work was funded by USGS grant G13AP00057. The conclusions presented here should not be interpreted as representing the opinion of the U.S. Geological Survey.

Abstract

Hosseini, Seyed Mehrdad. Ph.D. The University of Memphis. August 2014. Reducing uncertainties in the velocities determined by inversion of phase velocity dispersion curves using synthetic seismograms. Major Professor: Shahram Pezeshk.

Characterizing the near-surface shear-wave velocity structure using Rayleigh-wave phase velocity dispersion curves is widespread in the context of reservoir characterization, exploration seismology, earthquake engineering, and geotechnical engineering. This surface seismic approach provides a feasible and low-cost alternative to the borehole measurements. Phase velocity dispersion curves from Rayleigh surface waves are inverted to yield the vertical shear-wave velocity profile. A significant problem with the surface wave inversion is its intrinsic non-uniqueness, and although this problem is widely recognized, there have not been systematic efforts to develop approaches to reduce the pervasive uncertainty that affects the velocity profiles determined by the inversion. Non-uniqueness cannot be easily studied in a nonlinear inverse problem such as Rayleigh-wave inversion and the only way to understand its nature is by numerical investigation which can get computationally expensive and inevitably time consuming. Regarding the variety of the parameters affecting the surface wave inversion and possible non-uniqueness induced by them, a technique should be established which is not controlled by the non-uniqueness that is already affecting the surface wave inversion. An efficient and repeatable technique is proposed and tested to overcome the non-uniqueness problem; multiple inverted shear-wave velocity profiles are used in a wavenumber integration technique to generate synthetic time series resembling the geophone recordings. The similarity between synthetic and observed time series is used as an additional tool along with the similarity between the theoretical and experimental dispersion curves. The proposed method is proven to be effective through synthetic and real world examples. In these examples, the nature of the non-uniqueness is discussed and its existence is shown. Using the proposed technique, inverted velocity profiles are estimated and effectiveness of this technique is evaluated; in the synthetic example, final inverted velocity profile is compared with the initial target velocity model, and in the real world example, final inverted shear-wave velocity profile is compared with the velocity model from independent measurements in a nearby borehole. Real world example shows that it is possible to overcome the non-uniqueness and distinguish the representative velocity profile for the site that also matches well with the borehole measurements.

Table of Contents

List of Figures

Chapter 1. Introduction

Seismic design of structures depends on the realistic anticipation of the ground motions generated from various seismic sources. In the design process, seismic structural stability depends on the rate of seismic hazard for a specific region, and in recent years, engineers and seismologists have been working meticulously to correctly estimate the seismic hazard. Seismic hazard is defined as the response of the earth surface with respect to the ground motion of an earthquake. The seismic wave field generated at the location of the source travels though the earth's crust and reaches beneath the specific local site through the bedrock. Bedrock can be covered by deposits and geological structures with different materials and thicknesses. As the seismic wave field finds its way to the surface, passing through the heterogeneity of the local geology, it might get amplified and de-amplified. The greatest hazard is usually associated with soft deposits where seismic waves at the bedrock are amplified at certain frequency ranges as they reach the surface (Kramer, 1996). An example can be observed from the 2011 Tohoku M_w 9.0 earthquake, where seismic waves are recorded both at the bottom of a borehole and also on the surface at a station with a 320-km hypocentral distance. Figure 1.1 shows the three component seismograms of the surface and the borehole recorded at the station CHBH14 with the same scale. From this figure, it is evident that seismic waves are amplified as they reach the surface.

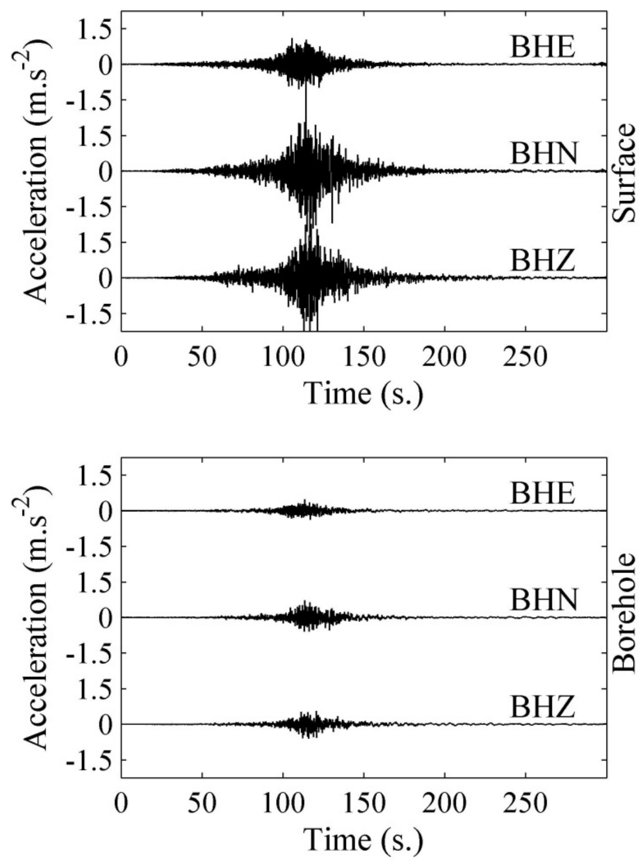

Figure 1.1. Three components of seismograms from 2011 Tohoku M_w 9.0 earthquake recorded on the surface (top) and also in depth of a borehole (bottom) in station CHBH14. The elevation difference between surface and borehole sensors is 525 meters. Seismic waves on the surface are amplified due to the local geology.

Site response correlates with the mechanical properties of the soil structure especially in its shallow depth. Among the various mechanical properties of soil, the shear-wave velocity (V_S) plays an important role in characterizing the site response.

The important effect of local geology is observed in sedimentary deposits in the Mississippi embayment area that significantly affect the ground motions in the probabilistic seismic-hazard maps. The reason is the possibility of amplification of seismic waves for certain frequency bands due to the shallow shear-wave velocity contrast between soft and stiff materials and soil behavior (Kramer, 1996; Pujol *et al*., 2002). The amplification of ground motion could adversely affect structures that resonate at periods similar to those of the ground on which they are built.

Reliable estimation of the shear-wave velocity profile is not only useful for site response studies and seismic hazard assessments, but is also of great interest in the context of other domains of engineering such as geotechnical engineering and petroleum engineering. In geotechnical engineering, V_S is used in the foundation design process as one of the properties of the underlying soil; in petroleum engineering, V_S is used for the noise attenuation in reflection sections, and for characterizing the near-surface velocity profiles.

1.1 Research Objective

The main objective of this dissertation is to provide a reliable and convenient method for estimation of the shear-wave velocity profile of the subsurface. Such a method will provide site-specific information in detail to improve the seismic hazard maps, specifically for the upper Mississippi embayment region. Soil conditions are often variable even inside of a relatively small area. Thus, to evaluate site-specific seismic hazard and to analyze site response in and around this region, it is necessary to find low-cost methods to obtain shear-wave velocity profiles. In general, borehole logging is considered to be the standard to obtain the needed soil dynamic properties; however, drilling and logging is expensive and this has led to the development of numerous inexpensive surface acquisition techniques. There are issues of non-uniqueness and uncertainties associated with non-invasive procedures that may not result in consistently reliable velocity profiles. Techniques used in this research are expected to improve the non-uniqueness issues in the estimated shear-wave velocity profiles from seismic surface methods, specifically those obtained by analyzing Rayleigh waves.

1.2 Research Overview

This project aims to improve near-surface characterization. A combination of techniques is used to reliably estimate the subsurface shallow shear-wave velocity profile. Currently, there are difficulties with such characterizations such as: (a) velocity reversals due to the presence of a low velocity layer, (b) the decrease in velocity with increasing depth, and (c) the depth of the water table. The problem with the last item is that the Poisson's ratio and density are different for dry and saturated materials. This fact has been usually neglected in the inversion of experimental dispersion curves, which is based on a layered model with small variations across the layers in the values of the Poisson's ratio and density. In fact, early papers on the subject state that the effect of changes in these two parameters is minimal (Nazarian, 1984; Nazarian & Stokoe, 1984). However, recent studies show that this may not be the case when a water table is present (Foti & Strobbia, 2002). In addition, the S-wave velocity models determined by the inversion of phase velocity dispersion curves are affected by a high degree of non-uniqueness because there is little absolute velocity information contained in the phase velocity. This lack of information causes the well-known velocity-depth trade-off (Ammon *et al*., 1990). For example, a thin layer with low velocity will produce an average differential arrival time similar to that caused by a thick layer with high velocity. As a consequence, the inverted velocity models depend on the initial velocity models or on the selected higher mode numbers, resulting in several different inverted velocity models. The proposed methodology helps distinguish among different velocity models by comparing their corresponding synthetic and observed time series.

1.3 Dissertation Overview

This dissertation is organized into six chapters and three appendices. Chapter two provides an overview of the estimation of the dispersive properties of surface waves. Chapter two first introduces basic wave propagation theory and unfolds the details of the propagator matrix technique, showing that it can be used for both seismogram synthesis and also theoretical phase velocity estimation in a heterogeneous media. Then, attenuation is presented and the mathematical techniques for implementation of attenuation in the synthesis theory are provided. It is shown how the dispersion is a necessity of a causal system, and some simulations are presented which will be used in development of future theories and assumptions for synthetic seismograms and comparison among observations and synthetics in future chapters.

Chapter three introduces the devices used in the MASW technique and unveils the details for a successful acquisition of surface waves. Common sources of error and uncertainties are introduced, including amplitude clipping and also the erroneous performance of the trigger which can adversely affect the reliability of results. At the end of Chapter three, the dispersion curve obtained by the MASW technique is compared with that from another surface seismic test (spectral analysis of surface waves, SASW) to see how close is the agreement of the two methods.

Chapter four sets forth the details of the calculation of the experimental dispersion curve from a recorded time series. This section discusses details of the frequency-wavenumber technique and sheds light on this signal processing method by synthetic and real examples. Chapter four also shows a technique to invert the experimental dispersion curve for the shear-wave velocity structure of the subsurface, and the formulation of the iterative Levenberg-Marquardt inversion is provided. Program SURF96 from Dr. Robert Herrmann (St. Louis University) is introduced, and it is shown how the source code and settings are customized for a successful inversion in shallow applications. A few “bash” scripts are provided and explained to make the suggested modifications practical and repeatable.

Chapter five introduces a synthetic example of the non-uniqueness in the inversion of surface waves, and demonstrates how easy it is to get confused among the pool of different inverted velocity profiles. To solve this problem, a synthetic seismogram technique is used to help separate the real representative profile from the other profiles.

Finally, Chapter six applies all of the techniques explained in the previous chapters to the surface wave data recorded at a site near Memphis, Tennessee, and navigates the reader through the multiple techniques and all the details leading to the detection of the most reliable inverted shear-wave velocity profile. At the end of this chapter, an independent and solid evaluation of the proposed technique is performed by comparing the final inverted profile with the result from a downhole seismic survey. In a second evaluation, the inverted profile is also compared with those from two seismic tests at two sites with similar geology. Previously, two groups of researchers investigated these two sites using borehole and surface wave measurements, and I found it quite useful to compare my outcome with their published results.

Chapter 2. Literature Review and Basics of Wave Propagation

Knowledge regarding the near-surface seismic velocities unveils information about the subsurface lithology that is not available from surface geological observations (Petrosino *et al.*, 2002). Elastic properties of subsurface materials shed light on factors affecting the wave propagation phenomena, and enables researchers to predict ground motion and ultimately seismic hazard for a local site. Specifically, attenuation and shear-wave velocity structure in the top 30 meters play an important role for the estimation of strong ground motion at a site by estimating the amplification of ground motions or "site effect" (Bard & Bouchan, 1980a, 1908b; Boore *et al.*, 1994; Borcherdt, 1994; Cramer *et al*., 2002; Electric and Power Research Institute [EPRI], 1993; Evans & Pezeshk, 1998; Frankel & Vidale, 1992; Kramer, 1996; Malagnini *et al*., 1995; Moczo, 1989; Pezeshk and Liu, 2001; Pezeshk & Zarrabi, 2005; Pezeshk *et al*., 1998).

In the context of soil mechanics and foundation engineering, the shear-wave velocity has a direct relationship with the N-value (Craig, 1992; Xia *et al*., 2003), and in reservoir engineering it helps characterize the near-surface properties more accurately and suppress ground roll noise from the reflection sections (Salama *et al*., 2013; Strobbia *et al*., 2010, 2011, 2012).

The shear-wave velocity profile is estimated by considering the dispersive properties of Rayleigh and Love waves in a vertically heterogeneous medium (Brune & Dorman, 1963; Dorman & Ewing, 1962; Wiggins *et al*., 1972) and systematic approaches are developed for the use of surface waves in the geophysical and geotechnical prospecting (Gucunski & Woods, 1991; Park *et al*., 1998a; Pezeshk & Zarrabi, 2005; Rix *et al*., 2001;

Stokoe & Nazarian, 1983). Such methods rely on the inversion of the observed phase velocities for the shear-wave velocity structure by either using a linearized least square inversion (Rix *et al*., 2001; Xia *et al*., 1999; Yuan & Nazarian, 1993), or using evolutionary techniques such as a genetic algorithm or a simulated annealing procedure (Beaty *et al*., 2002; Luke & Calderón-Macias, 2007; Pezeshk & Zarrabi, 2005; Ryden & Park, 2006; Yamanaka & Ishida, 1996; Zeng, 2011; Hosseini & Pezeshk, 2011a). In either case, due to the nonlinearity of the equations, a nontrivial model null space exists that causes non-unique solutions of the surface wave inversion (Aster *et al*., 2003; Backus & Gilbert, 1970) where different velocity profiles might have similar phase velocity dispersion curves. A null space is a set of solutions (m_0) that if added to initial solution m, the result of a specific function $f(m)$ does not change, i.e. $f(m+m_0)=f(m)$, such as $\sin(\pi/2+2\pi)=\sin(\pi/2)$ where 2π can be considered as the null space of the model in this case (Aster *et al*., 2003). Specifically, Backus and Gilbert (1970) state that there is no answer to the question that whether, in a nonlinear problem, there are alternative solutions significantly different from the available one. They clearly indicate that to investigate solutions of a non-unique problem, one must either search for solutions by numerical techniques, or use Monte Carlo methods introduced by Keilis-Borok and Yanovskaya (1967) and Levshin et al. (1966). Hence, in the nonlinear inversion of Rayleigh waves there is no objective way to discriminate among all the possible inversion results just by relying on the quality of fit between the observed and inverted dispersion data. Although the non-uniqueness is a well-known issue in surface wave inversion, there have not been systematic efforts to address the issue. Widely-used linearized inversion techniques seek iteratively for a solution that is linearly close to the initial model (Cercato, 2009; Parker, 1994) and does not search automatically for the whole solution space (Stovall, 2010). The degree of the non-uniqueness of the problem directly controls the possibility that the objective function contains the solution as a part of its local minima (Backus & Gilbert, 1970; Cercato, 2009), and there is no absolute treatment to handle such non-uniqueness. In a linearized inversion, several techniques have been proposed by researchers, such as imposing constraints on the velocity variations and inclusion of the higher modes (Cercato, 2007, 2009; Gabriels, 1987; Levshin & Panza, 2006; Park *et al*., 1999b; Stovall, 2010; Xia *et al*., 2003). Typically, higher modes are dominant in cases where a high velocity layer is present, or when the source-array offset increases (Cercato, 2009; Cercato *et al*., 2010; Stovall, 2010; Tokimatsu *et al*., 1992; Xia *et al*., 2002). In the inversion of dispersion data including higher modes, a correct identification of mode numbers is essential (Cercato, 2009; Cerato *et al*., 2010; Forbriger, 2003a, 2003b; Stovall, 2010; Hosseini & Pezeshk, 2011b, 2011c, 2011d, 2012a; Stovall et al. 2011).

Aforementioned techniques that deal with the non-uniqueness problem deal more with the numerical solutions that implements a larger portion of the dispersion data in the inversion process. Along with these techniques, there have been efforts to bring another source of verification by using synthetic time series. Malagnini (1996) and Malagnini et al. (1995) inverted dispersion curves from a shallow explosion, and verified the reliability of the inverted shear-wave velocity profile by comparing the observed and the associated synthetic time series. It has been proven that seismograms can hold information regarding the properties of soil layers, and in the context of seismology and exploration, there has been extensive research on the waveform inversion through which the compressional and shear-wave velocities, and in some cases, density of layers/cells are estimated (Strobbia *et al*., 2012; Zeng, 2011; Tran & Hiltunen, 2012; Groos, 2013).

In this study, a seismogram synthesis technique (Wang & Herrmann, 1980) is used to discriminate among several profiles emerging from the inversion of phase velocity dispersion curves obtained at a site near Memphis, Tennessee. Regarding the contrast between the embayment soft deposits and the surrounding firmer medium, the amplifying effect of the shallow soil profile is of great importance in the sedimentary deposits of Mississippi embayment (Cramer, 2006; Kramer, 1996; Pujol *et al.*, 2002; Taborda, 2013). The importance of an accurate estimation of the shear-wave velocity profile is in the site response analysis, while otherwise unsatisfactory and often dangerous results may emerge (Boaga *et al*., 2012). For this study, a multi-channel analysis of surface waves (MASW) (Park *et al*., 1999a; Xia *et al*., 1999a, 1999b) and a downhole seismic survey are conducted. Phase velocity dispersion data from the MASW test are inverted for several high resolution shear-wave velocity profiles, and then synthetic seismograms are used to find the velocity profile with a minimum error between the synthetics and the observed time series recorded at each surface geophone (Hosseini & Pezeshk, 2012b, 2012c). Then, the final shear-wave velocity profile from the seismogram match is compared with that from the downhole seismic survey, to validate the effectiveness of the proposed technique in identifying the most appropriate velocity profile among a pool of shear-wave velocity structures, inverted through a non-unique process.

In the next section, the equation of motion is introduced and details are provided on how the problem of the wave propagation in a homogeneous half-space is formulated, and how it contains compressional and transverse waves.

2.1 Equation of Motion

Considering small deformations, the strain tensor from Eulerian and Lagrangian descriptions becomes the same (Pujol, 2003) and the infinitesimal strain tensor can be expressed as:

$$\varepsilon_{kl} = \frac{1}{2}\left(u_{k,l} + u_{l,k}\right) \qquad (2.1)$$

where ε_{kl} is Cauchy's strain tensor, and $u_{i,j}$ is the derivative of displacement in direction *i* with respect to *j* direction. Hereafter, the comma sign means derivative with respect to the direction mentioned right after the comma. Also, the equation of motion can be approximated by neglecting spatial derivatives of *u* which becomes:

$$\tau_{ij,j} + \rho f_i = \rho \frac{\partial^2 u_i}{\partial t^2} = \rho \ddot{u}_i \qquad (2.2)$$

where τ_{ij} is the stress tensor holding normal and shearing stresses, ρ is the density of the medium, f is the body force per unit volume, *t* is the time, and finally double dots indicates a second derivative with respect to time. Equation (2.1) is Cauchy's equation of motion.

A three-dimensional representation of stress tensors on an infinitesimal cube is presented in Figure 2.1. It is very common to express a stress symbol with σ_{ii} when the direction of force and the normal axis of the plane that the stress acts on are in the same direction. It is common to distinguish the Cartesian axis with numbers 1, 2, and 3 indicating directions X, Y, and Z. Therefore, in symbol τ_{ij}, *i* and *j* can be replaced with numbers from 1 to 3, and with this convention τ_{ij} can represent any type of stress in the tensor:

$$\tau = \begin{bmatrix} \tau_{xx}(=\sigma_{xx}) & \tau_{xy} & \tau_{xz} \\ \tau_{yx} & \tau_{yy}(=\sigma_{yy}) & \tau_{yz} \\ \tau_{zx} & \tau_{zy} & \tau_{zz}(=\sigma_{zz}) \end{bmatrix} = \begin{bmatrix} \tau_{11} & \tau_{12} & \tau_{13} \\ \tau_{21} & \tau_{22} & \tau_{23} \\ \tau_{31} & \tau_{32} & \tau_{33} \end{bmatrix} \tag{2.3}$$

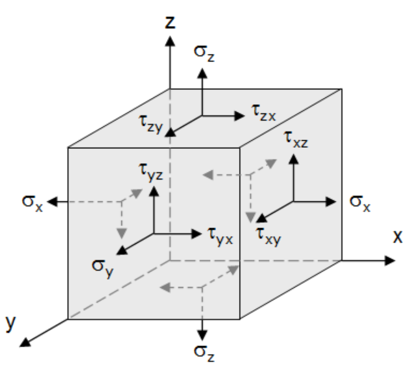

Figure 2.1. Stress tensor presented on an infinitesimal cube.

2.1.1 Strain-Stress Relationship and the Equation of Motion

Equation (2.1) relates displacement and strain, and Equation (2.2) relates the displacement with stress. By considering the approximation in deriving these sets of equations, they are valid for any continuous medium. To establish detailed behavior of the wave propagation in a specific medium, we should then introduce the relationship between stress and strain. Such a relationship is expressed using Hooke’s law, which relates the deformations to exerted forces. The generalized version of Hooke's law was established by Cauchy (Pujol, 2003; Timoshenko, 1953) as:

$$\tau_{kl} = c_{klpq}\varepsilon_{pq} \tag{2.4}$$

where c_{klpq} is the fourth-order tensor related to properties of the medium, and its reaction to different type of waves and different directions and positions. In general, c_{klpq} has 81 components which is reduced to 36 after considering the symmetry of stress and strain.

In earth sciences, the tensor c_{klpq} can be simplified even more by assumptions such as that the properties of the medium are the same in any direction (isotropic material). In such case, c_{klpq} for an isotropic solid reduces to:

$$c_{ijkl} = \lambda\delta_{ij}\delta_{kl} + \mu(\delta_{ik}\delta_{jl} + \delta_{il}\delta_{jk}) \tag{2.5}$$

where λ and μ are the Lamé constants, and δ_{ij} is the Kronecker delta function defined as:

$$\delta_{ij} = \begin{Bmatrix} 1 & \text{if } i = j \\ 0 & \text{if } i \neq j \end{Bmatrix} \tag{2.6}$$

Lamé constants are material properties and are related to other parameters for material properties in engineering and seismology. In seismology, shear and compressional wave velocities (V_P and V_S) are related to Lamé constants by the following equations:

$$V_P = \sqrt{\frac{\lambda + 2\mu}{\rho}} = \alpha$$
$$V_S = \sqrt{\frac{\mu}{\rho}} = \beta \tag{2.7}$$

In civil engineering, the bulk modulus (K), Young's Modulus (E), and the Poisson's ratio (ν) can be defined as:

$$\begin{gathered} E = \frac{\mu(3\lambda + 2\mu)}{\mu + \lambda} = \frac{\rho V_S^2 (3V_P^2 - 4V_S^2)}{V_P^2 - V_S^2} \\ K = \lambda + \frac{2}{3}\mu = \rho(V_P^2 - \frac{4}{3}V_S^2) \\ \nu = \frac{\lambda}{2(\lambda + \mu)} = \frac{V_P^2 - 2V_S^2}{2\left(V_P^2 - V_S^2\right)} \end{gathered} \tag{2.8}$$

To do more manipulations on the equation of motion, a series of mathematical operators are defined in Table 2.1.

Referring back to the Equation (2.4), the stress and strain relationship can be explicitly defined as:

$$\tau_{ij} = \lambda \delta_{ij} \varepsilon_{kk} + 2\mu \varepsilon_{ij} \tag{2.9}$$

Now we can use Equation (2.9) to rewrite the equation of motion (2.2) as:

$$\frac{\partial \tau_{ij}}{\partial x_j} + f_i = \rho \frac{\partial^2 u_i}{\partial t^2} \tag{2.10}$$

Table 2.1. Mathematical operators used in the study to set up the equation of motion

Operator Name	Equation
Differential Operator	$\nabla = \frac{\partial}{\partial x}\mathbf{e}_1 + \frac{\partial}{\partial y}\mathbf{e}_2 + \frac{\partial}{\partial z}\mathbf{e}_3$
Gradient	$\nabla f = \frac{\partial f}{\partial x}\mathbf{e}_1 + \frac{\partial f}{\partial y}\mathbf{e}_2 + \frac{\partial f}{\partial z}\mathbf{e}_3$
Divergence	$\nabla \cdot f = \frac{\partial f}{\partial x} + \frac{\partial f}{\partial y} + \frac{\partial f}{\partial z}$
Curl	$\nabla \times f = \begin{vmatrix} i & j & k \\ \frac{\partial}{\partial x} & \frac{\partial}{\partial y} & \frac{\partial}{\partial z} \\ f_x & f_y & f_z \end{vmatrix} = \left(\frac{\partial f_z}{\partial y} - \frac{\partial f_y}{\partial z}\right)\mathbf{e}_1 + \left(\frac{\partial f_x}{\partial z} - \frac{\partial f_z}{\partial x}\right)\mathbf{e}_2 + \left(\frac{\partial f_y}{\partial x} - \frac{\partial f_x}{\partial y}\right)\mathbf{e}_3$
Laplacian	$\nabla^2 f = \nabla \cdot \nabla f = \frac{\partial^2 f}{\partial x^2}\mathbf{e}_1 + \frac{\partial^2 f}{\partial y^2}\mathbf{e}_2 + \frac{\partial^2 f}{\partial z^2}\mathbf{e}_3$

In Table 2.1 definitions, $\mathbf{e}$ stands for the unit vector. By using Equations (2.9) and (2.1) and the definitions provided in Table 2.1, the equation of motion can be introduced in a vector format as:

$$\mu\nabla^2\mathbf{u} + (\lambda+\mu)\nabla(\nabla\cdot\mathbf{u}) + \rho\mathbf{f} = \rho\frac{\partial^2\mathbf{u}}{\partial t^2} \tag{2.11}$$

Expanding Equation (2.11) further using $\nabla^2\mathbf{u} = \nabla(\nabla\cdot\mathbf{u}) - \nabla\times(\nabla\times\mathbf{u})$, the equation of motion gets the following form:

$$\frac{(\lambda+\mu)}{\rho}\nabla(\nabla\cdot\mathbf{u}) - \frac{\mu}{\rho}\nabla\times\nabla\times\mathbf{u} + \mathbf{f} = \frac{\partial^2\mathbf{u}}{\partial t^2} \tag{2.12}$$

Finally, using Equation set (2.7), one will get the Navier's elastic wave equation:

$$\alpha^2\ \nabla(\nabla\cdot\mathbf{u})-\beta^2\ \nabla\times\nabla\times\mathbf{u}+\mathbf{f}=\frac{\partial^2\mathbf{u}}{\partial t^2}=\ddot{\mathbf{u}}\quad\text{(in time)}\tag{2.13}$$

$$\alpha^2\ \nabla(\nabla\cdot\mathbf{u})-\beta^2\ \nabla\times\nabla\times\mathbf{u}+\mathbf{f}=i\omega^2\mathbf{u}\quad\text{(in frequency)}\tag{2.14}$$

where the double dot on the right-hand side of Equation (2.13) means a second derivative with respect to time, and Equation (2.14) is in the frequency domain form. Note that Equation set (2.13) contains two type of propagating waves: dilatational (first term from left) and rotational (second term from left), corresponding to P and S waves. The equation of motion can also be presented as the following form, to match the notation of Ben-Menahem and Singh (1981, Section 4.1), for an applied force at depth z_0:

$$\begin{aligned}&\alpha^2\ \nabla(\nabla\cdot\mathbf{u})-\beta^2\ \nabla\times\nabla\times\mathbf{u}-\frac{\partial^2\mathbf{u}}{\partial t^2}=-\mathbf{S}_0 g(t)\delta(z-z_0)\qquad\text{(in time)}\\&\alpha^2\ \nabla(\nabla\cdot\mathbf{u})-\beta^2\ \nabla\times\nabla\times\mathbf{u}-i\omega^2\mathbf{u}=-\mathbf{S}_0 g(\omega)\delta(z-z_0)\quad\text{(in frequency)}\end{aligned}\tag{2.15}$$

where term $\mathbf{S}_0\, g(t)\ \delta(z\text{-}z_0)$ represents the body force per unit mass, which is a force of a specific magnitude in different directions ($\mathbf{S}_0$), concentrated at the depth $z=z_0$, and $g(t)$ is a dimensionless function time variation of the force, and $g(\omega)$ is the Fourier transform of $g(t)$. Displacement vector $\mathbf{u}$ which is the solution to Equation (2.15), can be expressed as (Pujol, 2003):

$$\mathbf{u}(\mathbf{r},t)=h(t-\mathbf{k}.\mathbf{r}/c)+g(t+\mathbf{k}.\mathbf{r}/c)\tag{2.16}$$

where h and g are functions that travel forward and backward in time, t is time, c is the propagation velocity, **r** is the vector of location, and k is defined as a unit vector ($|\mathbf{k}| = 1$) equal to ($k_x.\mathbf{x}$, $k_y.\mathbf{y}$, $k_z.\mathbf{z}$). Pujol (2003) noted that for a given value of t ,$\mathbf{u}(\mathbf{r},t)$ is constant for all locations (x, y, and z) that **k.r** is a constant value such as C. In such case, equation **k**.**r** = C is the wave front of plane waves presented by Equation (2.16). Therefore plane waves have a normal vector **k** which is called wavenumber vector defining the wave fronts.

2.1.2 Potentials

The wave equation in Equation set (2.13) can be studied in terms of the type of waves that it produces. It is convenient to apply divergence operator to the equation of motion (2.13):

$$\alpha^2\ \nabla\cdot\nabla(\nabla\cdot\mathbf{u}) - \beta^2\ \nabla\cdot\nabla\times\nabla\times\mathbf{u} + \mathbf{f}' = \frac{\partial^2(\nabla\cdot\mathbf{u})}{\partial t^2} \qquad (2.17)$$

where $\mathbf{f}'$ is the body force vector after divergence operator is applied to. Knowing that $\nabla\cdot\nabla\times\nabla\times\mathbf{u}$ equals zero, then one can define $\varphi = \nabla\cdot\mathbf{u}$ as the P wave potential since the divergence operator calculates the outward flux of a vector field from an infinitesimal volume around a given point, and Equation (2.17) reduces to the familiar form of a vibrating string:

$$
\begin{aligned}
&\alpha^2\ \nabla\cdot\nabla(\varphi)=\frac{\partial^2(\varphi)}{\partial t^2}\\
&\Rightarrow\ \nabla^2(\varphi)=\frac{1}{\alpha^2}\frac{\partial^2(\varphi)}{\partial t^2}
\end{aligned}
\tag{2.18}
$$

The same way, curl operator is applied to the Equation (2.15). At every point in the field, the curl of that field is represented by a vector. The attributes of this vector (the length and the direction) characterize the rotation at that point. Applying the curl operator to the equation of motion will result in:

$$
\alpha^2\ \nabla\times\nabla(\nabla\cdot\mathbf{u})-\beta^2\ \nabla\times\nabla\times\nabla\times\mathbf{u}+\hat{\mathbf{f}}=\frac{\partial^2(\nabla\times\mathbf{u})}{\partial t^2}
\tag{2.19}
$$

where $\hat{\mathbf{f}}$ is the body force vector after the divergence operator. Knowing that $\nabla\times\nabla(\nabla\cdot\mathbf{u})$ equals zero, and that $\nabla\times\nabla\times\mathbf{X}=\nabla\times\nabla\cdot\mathbf{X}-\nabla\cdot\nabla\cdot\mathbf{X}$ for every vector **X**, then Equation (2.19) reduces to:

$$
\beta^2\ \nabla.\nabla(\nabla\times\mathbf{u})=\frac{\partial^2(\nabla\times\mathbf{u})}{\partial t^2}
\tag{2.20}
$$

and after defining $\boldsymbol{\psi}=\nabla\times\mathbf{u}$ as the S wave potential, an equation similar to the P wave potential will be obtained as:

$$
\nabla^2(\boldsymbol{\psi})=\frac{1}{\beta^2}\frac{\partial^2(\boldsymbol{\psi})}{\partial t^2}
\tag{2.21}
$$

The curl operator is a vector operator that describes the infinitesimal rotation of a three-dimensional vector field.

Based on the discussion above, the general equation of motion possesses two types of propagating waves at the same time, one moving in the direction of the propagation (φ potential), and one moving in the perpendicular direction of the propagation ($\boldsymbol{\psi}$ potential). The φ potential was obtained using the divergence operator and is related to P waves propagating with the speed of α. In the same way for the $\boldsymbol{\psi}$ potential, it was obtained using the curl operator and is related to S waves propagating with the speed of β. It is possible to show that the $\boldsymbol{\psi}$ potential can be decomposed further into two normal directions (each still perpendicular to the direction of the propagation, i.e., SH and SV). Interested readers can find more details on the topic in Aki and Richards (1980), Ben-Menahem and Singh (1981), and Pujol (2003).

Solving Equation (2.13) for a homogeneous half-space (where the material property does not change in any direction) has been studied in detail (Aki & Richards, 1980; Ben-Menahem & Singh, 1981). However, earth usually is considered as layers stacked on top of each other, where the property of material is the same in the horizontal direction and only changes with depth (z). The equation of motion in a multi-layered earth system is introduced in the next section, and important aspects of heterogeneity are presented.

2.1.3 Surface Waves in Heterogeneous Media

As mentioned before, the equation of motion (Equation 2.13) carries all components of motion. These components can be broken down into deformation in the direction of the wave propagation (x_1), and perpendicular to the propagation direction (x_2 and x_3). These displacements are referred to respectively as P, SV, and SH waves, and can be studied in term of potentials (Aki & Richards, 1980). In this study, the direction of the x_3 axis (z in Cartesian and z in spherical coordinates) is downward, the direction of the x_1 axis (z in Cartesian and r in spherical coordinates) is horizontal to the right, and the direction of the x_2 axis (y in Cartesian and θ in spherical coordinates) is perpendicular to the plane of x_1 and x_2 axes.

On the surface of a heterogeneous half-space, a series of waves are generated that attenuate with depth and are called surface waves. There are two types of surface waves: Rayleigh waves and Love waves. Rayleigh waves have an elliptical motion and are the result of the interaction between P and SV components. Love waves exist due to the SH component of the motion. The equation of motion can be analyzed further by making assumptions for deformation functions for displacements in different directions. For non-zero displacements, it can be shown that the solution to Equation (2.13) can be expressed in the following oscillatory format:

$$u(\mathbf{x},t) = \mathbf{A}e^{i(\omega t-\mathbf{kx})} \tag{2.22}$$

where **x** and **k** are the position and the wavenumber vectors. It should be noted that vector **A** represents the direction of ground motion and vector **k** represents the direction of propagation. Graphical representations of deformations due to the propagation of Rayleigh and Love waves are presented in Figure 2.2.

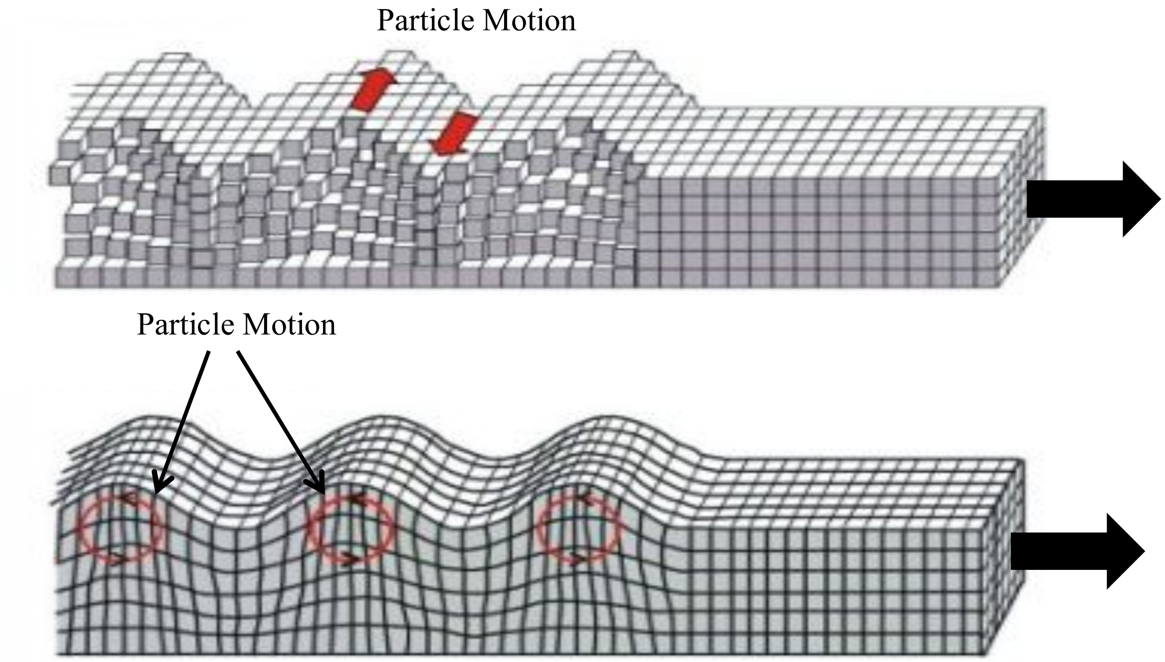

Figure 2.2. Particle motion caused by Love (top) and Rayleigh (bottom) surface waves (from Kramer, 1996).

2.1.3.1 Love Waves

System of coordination for writing the solution of equation of motion is defined as x ($x1$) in horizontal to the right direction, z ($x3$) is defined vertical downward direction, and y ($x2$) is defined perpendicular to the paper inward direction. Knowing that Love waves have deformation only in the x_2 direction, then Love deformations can be expressed as:

$$\begin{aligned} u_x &= 0 \\ u_y &= l_1(k, z, w)\exp\left[i(kx - \omega t)\right] \\ u_z &= 0 \end{aligned} \tag{2.23}$$

Please note that Equation set (2.28) is providing components of the displacement vector satisfying equation of motion in Equation (2.15) and is presented as $\mathbf{u} = u_x\mathbf{e}_1 + u_y\mathbf{e}_2 + u_z\mathbf{e}_3$. From Equation (2.23), stress components associated with the above deformations are:

$$\begin{aligned}
&\tau_{xx} = \tau_{yy} = \tau_{zz} = \tau_{zx} \\
&\tau_{yz} = \mu \frac{dl_1}{dz} \exp\left[i\left(kx - \omega t\right)\right] \\
&\tau_{xy} = ik\mu l_1 \exp\left[i\left(kx - \omega t\right)\right]
\end{aligned} \tag{2.24}$$

Substituting Equations (2.23) and (2.24) into Equation (2.2) will result in:

$$-\omega^2 \rho(z) l_1 = \frac{d}{dz}\left[\mu(z)\frac{dl_1}{dz}\right] - k^2 \mu(z) l_1 \tag{2.25}$$

Here, by introducing a new argument l_2, Equation (2.23) can be re-written as:

$$\tau_{yz} = l_2\left(k, z, w\right)\exp\left[i\left(kx - \omega t\right)\right] \tag{2.26}$$

Finally, the first-order differential Equations (2.25) and (2.26) can be expressed in a matrix form for the Love waves:

$$\frac{d}{dz}\begin{pmatrix} l_1 \\ l_2 \end{pmatrix} = \begin{pmatrix} 0 & \mu(z)^{-1} \\ k^2\mu(z) - \omega^2\rho(z) & 0 \end{pmatrix}\begin{pmatrix} l_1 \\ l_2 \end{pmatrix} \tag{2.27}$$

Equation (2.26) provides a relationship for the motion-stress vector inside a medium with material properties changing with depth.

2.1.3.2 Rayleigh Waves

The system of coordination is defined similar to the case of Love waves in the previous section. Similar to the previous section, one can express the following relationship for a Rayleigh waves motion-stress vector by defining the following displacement vectors:

$$\begin{aligned} u_x &= r_1(k,z,w)\exp\left[i(kx-\omega t)\right] \\ u_y &= 0 \\ u_z &= ir_2(k,z,w)\exp\left[i(kx-\omega t)\right] \end{aligned} \tag{2.28}$$

Please note that Equation set (2.28) is providing components of the displacement vector satisfying equation of motion in Equation (2.15) and is presented as $\mathbf{u}=u_x\mathbf{e}_1+u_y\mathbf{e}_2+u_z\mathbf{e}_3$. From Equation (2.28) and (2.2), stress components are calculated as:

$$
\begin{aligned}
\tau_{yz} &= \tau_{xy} = 0 \\
\tau_{xx} &= i\left[\lambda \frac{dr_2}{dz} + k(\lambda+2\mu)r_1\right]\exp\left[i\left(kx-\omega t\right)\right] \\
\tau_{yy} &= i\left[\lambda \frac{dr_2}{dz} + k\lambda r_1\right]\exp\left[i\left(kx-\omega t\right)\right] \\
\tau_{zz} &= i\left[(\lambda+2\mu)\frac{dr_2}{dz} + k\lambda r_1\right]\exp\left[i\left(kx-\omega t\right)\right] \\
\tau_{zx} &= \mu\left[\frac{dr_1}{dz} - kr_2\right]\exp\left[i\left(kx-\omega t\right)\right]
\end{aligned}
\tag{2.29}
$$

Since stress components τ_{zx} and τ_{zz} are continuous in the z direction, one can rewrite them as a function of two new terms:

$$
\begin{aligned}
\tau_{zx} &= r_3\left(k,z,w\right)\exp\left[i\left(kx-\omega t\right)\right] \\
\tau_{zz} &= ir_4\left(k,z,w\right)\exp\left[i\left(kx-\omega t\right)\right]
\end{aligned}
\tag{2.30}
$$

In Equation (2.28), the imaginary *i* factor is introduced in the vertical displacement to account for the π/2 shift, with the horizontal displacement modeling the elliptical motion of Rayleigh waves. The differential equations for the motion-stress vector $(r_1\ r_2\ r_3\ r_4)^T$ are obtained from Equations (2.28) to (2.30):

$$
\frac{d}{dz}\begin{pmatrix} r_1 \\ r_2 \\ r_3 \\ r_4 \end{pmatrix} = \begin{pmatrix} 0 & k & \mu^{-1}(z) & 0 \\ -k\lambda(z)\left[\lambda(z)+2\mu(z)\right]^{-1} & 0 & 0 & \left[\lambda(z)+2\mu(z)\right]^{-1} \\ k^2\xi(z)-\omega^2\rho(z) & 0 & 0 & k\lambda(z)\left[\lambda(z)+2\mu(z)\right]^{-1} \\ 0 & -\omega^2\rho(z) & -k & 0 \end{pmatrix}\begin{pmatrix} r_1 \\ r_2 \\ r_3 \\ r_4 \end{pmatrix}
\tag{2.31}
$$

where $\xi(z) = 4\mu(z)[\lambda(z) + \mu(z)] / [\lambda(z) + 2\mu(z)]$. The above equation in presented in Aki and Richards (1980) [AR80] and Ben-Menahem and Singh (1981) [BS81]. Care should be taken in comparing the two notations since the order of variable are different:

$$\begin{pmatrix} r_1 \\ r_2 \\ r_3 \\ r_4 \end{pmatrix}_{AR80} = \begin{pmatrix} y_1 \\ y_3 \\ y_2 \\ y_4 \end{pmatrix}_{BS81} \tag{2.32}$$

2.1.4 Dispersion of Rayleigh Waves and Synthetic Seismogram

This study only focuses on Rayleigh waves. In this section, a systematic approach is introduced to analyze displacements and tractions in a heterogeneous half-space for the combined effect of P and SV waves. The dispersive properties of a heterogeneous half-space medium can also be calculated as a secondary result of the analysis. Boundary conditions for Rayleigh waves is zero traction at the surface and zero displacement at the infinite depth:

$$\begin{aligned} &r_3, r_4 \to 0 \quad \text{as } z = 0 \text{ (free surface)} \\ &r_1, r_2 \to 0 \quad \text{as } z \to \infty \end{aligned} \tag{2.33}$$

Equation (2.31) is in the form of:

$$\frac{d\mathbf{f}(z)}{dz} = \mathbf{A}(z)\mathbf{f}(z) + \mathbf{s}\delta(z - z_0) \tag{2.34}$$

where $\mathbf{f}(z)=[r_1\ r_2\ r_3\ r_4]^{\mathrm{T}}$ is the motion-stress vector for a specific layer and $\mathbf{s}=[s_1^R\ \ s_2^R\ \ s_3^R\ \ s_4^R]$. There are two methods to deal with Equation (2.34): (1) to solve the inhomogeneous Equation (2.31); or (2) to solve the homogeneous version of (2.34) by putting $\mathbf{s}=0$, and applying the following source condition:

$$\mathbf{f}(z+0)-\mathbf{f}(z-0)=\mathbf{s} \tag{2.35}$$

The latter method avoids the direct calculation of the complicated parameters (Ben-Menahem & Singh, 1981) which follows in the rest of this section.

In Equation (2.34), matrix $\mathbf{A}(z)$ is a 4 by 4 matrix in the (x,z) plane (for the case of Rayleigh waves as in Equation 2.30) and is a 2 by 2 matrix (for the case of Love waves as in Equation 2.26). Matrix $\mathbf{A}(z)$ is constant for each isotropic layer in a heterogeneous system at a fixed depth. Using the Jordan decomposition of the motion-stress vector $\mathbf{f}(z)$ (Gantmatcher 1960; Turnbull & Aitken 1952), it is possible to rewrite it for Rayleigh waves as in Wang and Herrmann (1980):

$$\mathbf{f}(z)=\mathbf{Fw}=\mathbf{F}\begin{pmatrix}\mathrm{P_u}\\ \mathrm{S_u}\\ \mathrm{P_d}\\ \mathrm{S_d}\end{pmatrix} \tag{2.36}$$

where $\mathbf{w}$ is the wave-vector containing up-going and down-going wave types. The reason to decompose the motion stress vector $\mathbf{f}(z)$ to up going and down going waves is that some of the boundary conditions in heterogeneous media are imposed by suppressing certain type of waves at infinity $(z\rightarrow\infty)$, not just by limitations on the stress and strains. Therefore, motion-stress vector should be decomposed in the way introduced in Equation (2.36) and relate it to the wave-vector so the boundary conditions can be applied. Matrix **F** is made up from eigenvectors of **A**(z) times a matrix containing the vertical phase vectors (Aki & Richards, 1980):

$$\mathbf{F} = \mathbf{E}\boldsymbol{\Lambda}(z)$$
$$\mathbf{E} = \omega^{-1}\begin{pmatrix} \alpha k & \beta\nu & \alpha k & \beta\nu \\ \alpha\gamma & \beta k & -\alpha\gamma & -\beta k \\ -2\alpha\mu k\gamma & -\beta\mu(k^2+\nu^2) & 2\alpha\mu k\gamma & \beta\mu(k^2+\nu^2) \\ -\alpha\mu(k^2+\nu^2) & -2\beta\mu k\gamma & -\alpha\mu(k^2+\nu^2) & -2\beta\mu k\gamma \end{pmatrix} \tag{2.37}$$
$$\boldsymbol{\Lambda}(z) = \begin{pmatrix} e^{-\gamma z} & 0 & 0 & 0 \\ 0 & e^{-\nu z} & 0 & 0 \\ 0 & 0 & e^{\gamma z} & 0 \\ 0 & 0 & 0 & e^{\nu z} \end{pmatrix}$$

where $\nu = \sqrt{k^2 - \omega^2 / \beta^2}$ and $\gamma = \sqrt{k^2 - \omega^2 / \alpha^2}$, and therefore, the final form can be obtained:

$$\mathbf{f}(z) = \mathbf{E}\boldsymbol{\Lambda}(z)\mathbf{w} \tag{2.38}$$

In a layered media, there are motion-stress vectors **f**(z) for each layer as a function of depth (z) for the same layer. Motion-stress vectors connect to each other at different layers by the boundary conditions and assumption of tractions and displacements continuity at the interface between the layers. Therefore, if one starts from a specific layer and is able to move (recalculate) the motion-stress vector **f**(z) to a different depth in any layer, then the problem of finding the displacement in a heterogeneous half-space (synthesis of seismogram) is complete in frequency and wavenumber domain.

It will be shown that if no source of energy (external displacement or traction) is considered in such an approach, then one can find the pair of matching frequency-wavenumber through the process which yields the theoretical Rayleigh wave dispersion curve. Synthesis of seismogram goes a step further when a source of energy in an arbitrary depth can be implemented in the process of moving the motion-stress vector (as described above), and yield vertical and horizontal displacements which later are inverse-transformed into time and space domains.

A schematic view of the above concept is presented in Figure 2.3, in terms of involved matrices. Some of the matrices are not introduced yet, but will be introduced later.